Measurement range enlargement in Brillouin optical correlation-domain reflectometry based on double-modulation scheme

Yosuke Mizuno, Zuyuan He, and Kazuo Hotate*

Department of Electrical Engineering and Information Systems, The University of Tokyo, 7-3-1 Hongo, Bunkyo-ku, Tokyo 113-8656, Japan
**hotate@sagnac.t.u-tokyo.ac.jp*

Abstract: We have demonstrated a double-modulation scheme to enlarge the measurement range of Brillouin optical correlation-domain reflectometry for fiber-optic distributed strain sensing. In this scheme, the frequency of the laser output is simultaneously modulated with two different frequencies. In the experiment, 53-cm resolution and 1.5-km measurement range were simultaneously obtained. Furthermore, 27-cm resolution and 1.5-km measurement range were also simultaneously achieved when a noise-floor compensation technique was employed.

OCIS codes: (060.2370) Fiber optics sensors; (280.4788) Optical sensing and sensors; (290.5830) Scattering, Brillouin.

References and links

1. Y. Mizuno, W. Zou, Z. He, and K. Hotate, "Proposal of Brillouin optical correlation-domain reflectometry (BOCDR)," Opt. Express **16**(16), 12148–12153 (2008).
2. Y. Mizuno, Z. He, and K. Hotate, "One-end-access high-speed distributed strain measurement with 13-mm spatial resolution based on Brillouin optical correlation-domain reflectometry," IEEE Photon. Technol. Lett. **21**(7), 474–476 (2009).
3. A. Fellay, L. Thevenaz, M. Facchini, M. Nikles, and P. Robert, "Distributed sensing using stimulated Brillouin scattering: towards ultimate resolution," *Proc. 12th Intern. Conf. Optical Fiber Sensors*, 324–327 (1997).
4. T. Kurashima, T. Horiguchi, H. Izumita, S. Furukawa, and Y. Koyamada, "Brillouin optical-fiber time domain reflectometry," IEICE Trans. Commun," E **76-B**, 382–390 (1993).
5. T. Horiguchi and M. Tateda, "BOTDA-nondestructive measurement of single-mode optical fiber attenuation characteristics using Brillouin interaction: theory," J. Lightwave Technol. **7**(8), 1170–1176 (1989).
6. Y. Koyamada, Y. Sakairi, N. Takeuchi, and S. Adachi, "Novel technique to improve spatial resolution in Brillouin optical time-domain reflectometry," IEEE Photon. Technol. Lett. **19**(23), 1910–1912 (2007).
7. W. Li, X. Bao, Y. Li, and L. Chen, "Differential pulse-width pair BOTDA for high spatial resolution sensing," Opt. Express **16**(26), 21616–21625 (2008).
8. Y. Mizuno, Z. He, and K. Hotate, "Measurement range enlargement in Brillouin optical correlation-domain reflectometry based on temporal gating scheme," Opt. Express **17**(11), 9040–9046 (2009).
9. K. Hotate, and T. Hasegawa, "Measurement of Brillouin gain spectrum distribution along an optical fiber using a correlation-based technique – proposal, experiment and simulation," IEICE Trans. Electron E **83-C**, 405–412 (2000).
10. K. Hotate, and M. Tanaka, "Correlation-based continuous-wave technique for optical fiber distributed strain measurement using Brillouin scattering with cm-order spatial resolution – applications to smart materials," IEICE Trans. Electron E **84-C**, 1823–1828 (2001).
11. G. P. Agrawal, Nonlinear Fiber Optics (Academic Press, California, 1995).
12. T. Horiguchi, T. Kurashima, and M. Tateda, "Tensile strain dependence of Brillouin frequency shift in silica optical fibers," IEEE Photon. Technol. Lett. **1**(5), 107–108 (1989).
13. T. Kurashima, T. Horiguchi, and M. Tateda, "Thermal effects on the Brillouin frequency shift in jacketed optical silica fibers," Appl. Opt. **29**(15), 2219–2222 (1990).
14. K. Y. Song, Z. He, and K. Hotate, "Distributed strain measurement with millimeter-order spatial resolution based on Brillouin optical correlation domain analysis," Opt. Lett. **31**(17), 2526–2528 (2006).
15. Y. Mizuno, Z. He, and K. Hotate, "Stable entire-length measurement of fiber strain distribution by Brillouin optical correlation-domain reflectometry with polarization scrambling and noise-floor compensation," Appl. Phys. Express **2**, 062403 (2009).
16. Y. Ohtsuka, "Optical coherence effects on a fiber-sensing Fabry-Perot interferometer," Appl. Opt. **21**(23), 4316–4320 (1982).
17. A. W. Brown, M. D. DeMerchant, X. Bao, and T. W. Bremner, "Spatial resolution enhancement of a Brillouin-distributed sensor using a novel signal processing method," J. Lightwave Technol. **17**(7), 1179–1183 (1999).

#121173 - $15.00 USD Received 8 Dec 2009; revised 1 Mar 2010; accepted 3 Mar 2010; published 10 Mar 2010

18. M. P. Song, and B. Zhao, "Accuracy enhancement in Brillouin scattering distributed temperature sensor based on Hilbert transform," Opt. Commun. **250**(4-6), 252–257 (2005).

1. Introduction

Among various kinds of fiber-optic sensors, Brillouin optical correlation-domain reflectometry (BOCDR) [1] has the capacity to measure the distribution of strain and/or temperature along a fiber under test (FUT) from a single end. So far, 13-mm spatial resolution has been obtained in a silica fiber [2], which is the best result ever reported in spontaneous Brillouin scattering-based reflectometers. However, BOCDR suffers from a trade-off between the measurement range and the spatial resolution. Their ratio N_R is fixed at approximately 570 due to the limitation caused by Rayleigh scattering-induced noise [1]. For example, when the spatial resolution is set to 40 cm or 13 mm, the measurement range becomes 224 m [1] or 7.6 m [2], respectively. Thus, in order to achieve kilometer-order measurement range, the resolution must be 2 m or larger, which is even worse than that of basic time-domain techniques (~1 m [3]), such as Brillouin optical time-domain reflectometry (BOTDR) [4] and Brillouin optical time-domain analysis (BOTDA) [5]. In the time-domain systems, some progress has also been made to enhance the resolution [6]-[7].

To obtain higher N_R, a temporal gating scheme was implemented [8], where any correlation peak within the FUT can be arbitrarily selected by a time-domain technique. In the experiment, 66-cm resolution and 1-km measurement range were simultaneously achieved. The ratio N_R was 1515, which is about three times as high as that of the basic BOCDR. However, the signal-to-noise (S/N) ratio was so low that N_R could not be enhanced further.

In the case of Brillouin optical correlation-domain analysis (BOCDA) systems [9], a multiple-modulation scheme is known to be an alternative method to obtain higher N_R [10], where the frequency of the laser output is simultaneously modulated with multiple different frequencies. In the previous experiment, by modulating the laser output at $2f_0$ and $3f_0$ simultaneously (where f_0 is a fundamental frequency), N_R was enhanced by three times.

In this paper, we demonstrate a double-modulation scheme to enlarge the measurement range of BOCDR while maintaining the spatial resolution. The optimized modulation parameters are described, such as the combination of the frequencies to be used, and their amplitudes. Then, the operating principle of the scheme is theoretically analyzed and simulated. In the experiment, a strain-applied 90-cm section is successfully detected with 53.1-cm resolution and 1.51-km measurement range (N_R = 2845). Moreover, a strain-applied 40-cm section is also detected with 26.5-cm resolution and 1.51-km measurement range (N_R = 5690) by the use of a noise-floor compensation technique.

2. Principle

Spontaneous Brillouin scattering occurs when light is Bragg-reflected by the refractive index modulations produced by acoustic phonons. Since the phonons decay exponentially, the backscattered Brillouin light (Stokes light) spectrum, also known as Brillouin gain spectrum (BGS), takes the shape of a Lorentzian function [11]. The Stokes light suffers a Doppler shift called Brillouin frequency shift (BFS), which depends on tensile strain and temperature change applied to the optical fiber. For example, in a standard silica single-mode fiber (SMF), BFS of about 11 GHz slightly varies to higher frequency in proportion to the applied strain and the temperature change with coefficients of 0.058 MHz/με [12] and 1.18 MHz/K [13], respectively. Hence, BFS can provide the information on the magnitude of strain and temperature change in the fiber.

BOCDR [1] is a technology to measure the distribution of strain and/or temperature along an FUT from a single end, based on the correlation control of continuous lightwaves. The Stokes light due to the spontaneous Brillouin scattering of the pump light in the FUT is heterodyned with the reference light (self heterodyne). In order to resolve the strain-applied position, the pump light and the reference light are sinusoidally frequency-modulated, producing periodical correlation peaks along the FUT. The measurement range d_m, that is, the interval of the correlation peaks, and the spatial resolution Δz are given by:

#121173 - $15.00 USD Received 8 Dec 2009; revised 1 Mar 2010; accepted 3 Mar 2010; published 10 Mar 2010

$$d_{\mathrm{m}} = \frac{c}{2n f_{\mathrm{mod}}}, \tag{1}$$

$$\Delta z = \frac{c\Delta \nu_{B}}{2\pi n f_{\mathrm{mod}} \Delta f}, \tag{2}$$

respectively, where c is the velocity of light, n the refractive index, f_{mod} the modulation frequency of the light source, $\Delta \nu_{\mathrm{B}}$ the Brillouin gain bandwidth in optical fibers, and Δf the modulation amplitude of the light source. The number of effective sensing points N_{R}, which can be regarded as the evaluation parameter of the system, is given by the ratio between d_{m} and Δz, as:

$$N_{\mathrm{R}} = \frac{d_{\mathrm{m}}}{\Delta z} = \frac{\pi \Delta f}{\Delta \nu_{\mathrm{B}}}. \tag{3}$$

According to Eq. (3), Δf needs to be increased to obtain higher N_{R}. Although Δf is not limited in BOCDA [14], Δf must be lower than a half of BFS in the fiber in BOCDR [1], which results in N_{R} lower than about 570 for standard silica fibers.

Another way to achieve higher N_{R} is to utilize multiple intervals of the correlation peaks. In this case, we select only one correlation peak for a distributed measurement, but suppress other peaks to avoid the crosstalk. Therefore, the measurement range is multiplied while the spatial resolution is maintained. Along with the temporal gating scheme [8], the double-modulation scheme is an effective method for this purpose, and was applied to BOCDA [10].

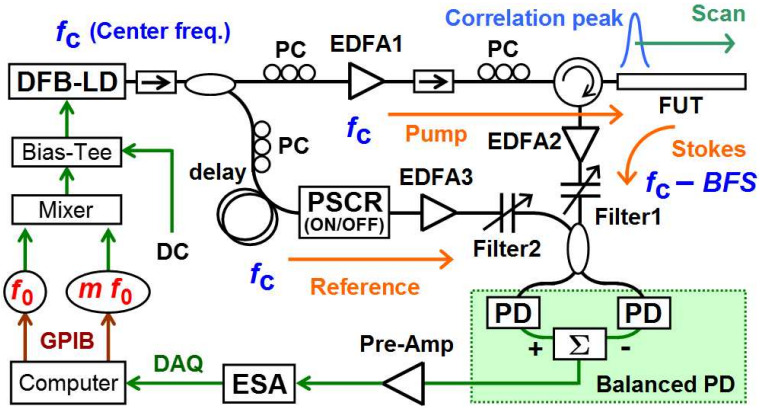

Fig. 1. Experimental setup of BOCDR based on double-modulation scheme: DAQ, data acquisition; DC, direct current; EDFA, erbium-doped fiber amplifier; ESA, electrical spectrum analyzer; FUT, fiber under test; GPIB, general-purpose interface bus; PC, polarization controller; PD, photo-detector; PSCR, polarization scrambler.

The experimental setup of BOCDR based on the double-modulation scheme is depicted in Fig. 1. The roles of each device including the polarization scrambler (PSCR) and the optical filters are the same as described in [15]. The pump light and the reference light are sinusoidally frequency-modulated with two different frequencies, f_0 ($+f_\varepsilon$) and $m f_0$, where f_0 is a fundamental frequency, m is an integer, and f_ε (~0.5 kHz) is needed to avoid beating between the two frequencies, which causes large fluctuations of BGS. The amplitude of the frequency modulation at f_0, denoted as Δf_1, is set to be several hundreds of MHz (difficult to measure accurately due to the frequency characteristics of the laser circuit). The amplitude at $m f_0$, denoted as Δf_{m}, is about 5.4 GHz (a little lower than a half of BFS in silica fibers). Then, as shown in Fig. 2, the spatial resolution is determined by $m f_0$, while the correlation peaks of which the orders are not multiples of m are suppressed by f_0. Since the modulation at f_0 does not influence on the resolution due to the low Δf_1, it becomes possible to achieve the spatial

#121173 - $15.00 USD Received 8 Dec 2009; revised 1 Mar 2010; accepted 3 Mar 2010; published 10 Mar 2010

resolution determined by $m f_0$ and the measurement range determined by f_0 simultaneously, leading to a larger N_R by m times.

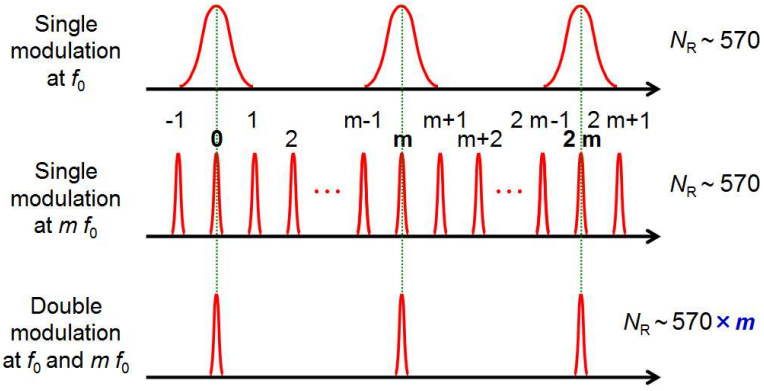

Fig. 2. Operating principle of double-modulation scheme.

3. Theoretical analysis and simulation

The operating principle of the double-modulation scheme was theoretically analyzed. The frequency modulation of the laser output is represented as Eq. (4):

$$f(t) = f_c + \Delta f_m \sin(2\pi m f_0 t) + \Delta f_1 \sin(2\pi f_0 t), \tag{4}$$

where is the center frequency. Then, the electric field of the laser output is expressed as Eq. (5):

$$E(t) = \exp\{-j\Phi(t)\}, \tag{5}$$

where $\Phi(t)$ is defined by Eq. (6):

$$\Phi(t) = \int_0^t 2\pi f(t')\,dt'. \tag{6}$$

It is known that the optical coherence function, which is the shape of the correlation peaks along the FUT, is given by the Fourier transform of the spectral density of the light source, or in other words, the autocorrelation function of the electric field of the light source [16]. Therefore, the absolute value of the optical coherence function is calculated as

$$|\gamma(\tau_d)| = \left| \lim_{T\to\infty} \frac{1}{T} \int_{-\frac{T}{2}}^{\frac{T}{2}} \exp\{-j\Phi(t)\} \exp\{j\Phi(t-\tau_d)\}\,dt \right|$$

$$= \left| \lim_{T\to\infty} \frac{1}{T} \int_{-\frac{T}{2}}^{\frac{T}{2}} \exp\left[j\left\{ -2\pi f_c \tau_d + 2\frac{\Delta f_m}{m f_0} \sin(\pi m f_0 \tau_d) \sin\left(2\pi m f_0 \left(t - \frac{\tau_d}{2}\right)\right) \right.\right.\right.$$

$$\left.\left.\left. + 2\frac{\Delta f_1}{f_0} \sin(\pi f_0 \tau_d) \sin\left(2\pi f_0 \left(t - \frac{\tau_d}{2}\right)\right) \right\} \right] dt \right|$$

$$= \left| \lim_{T\to\infty} \frac{1}{T} \int_{-\frac{T}{2}}^{\frac{T}{2}} \sum_{p=-\infty}^{\infty} J_p\left(2\frac{\Delta f_m}{m f_0} \sin(\pi m f_0 \tau_d)\right) \exp\left\{ j2\pi p m f_0 \left(t - \frac{\tau_d}{2}\right) \right\} \right.$$

$$\left. \cdot \sum_{q=-\infty}^{\infty} J_q\left(2\frac{\Delta f_1}{f_0} \sin(\pi f_0 \tau_d)\right) \exp\left\{ j2\pi q f_0 \left(t - \frac{\tau_d}{2}\right) \right\} dt \right|$$

#121173 - $15.00 USD Received 8 Dec 2009; revised 1 Mar 2010; accepted 3 Mar 2010; published 10 Mar 2010

$$= \left| \lim_{T\to\infty} \frac{1}{T} \int_{-\frac{T}{2}}^{\frac{T}{2}} \sum_{p=-\infty}^{\infty} \sum_{q=-\infty}^{\infty} J_p\left(2\frac{\Delta f_m}{mf_0}\sin(\pi m f_0 \tau_d)\right) \cdot J_q\left(2\frac{\Delta f_1}{f_0}\sin(\pi f_0 \tau_d)\right) \right.$$
$$\left. \cdot \exp\left\{ j2\pi(pm+q) f_0 \left(t - \frac{\tau_d}{2}\right)\right\} dt \right|$$
$$= \left| \sum_{p=-\infty}^{\infty} J_p\left(2\frac{\Delta f_m}{mf_0}\sin(\pi m f_0 \tau_d)\right) \cdot J_{-pm}\left(2\frac{\Delta f_1}{f_0}\sin(\pi f_0 \tau_d)\right) \right|, \quad (7)$$

where τ_d is the time delay and $J_p(x)$ is the p-th Bessel function of the first kind. When $m >> 1$, Eq. (7) is approximately equal to Eq. (8):

$$|\gamma(\tau_d)| \approx \left| J_0\left(2\frac{\Delta f_m}{mf_0}\sin(\pi m f_0 \tau_d)\right)\right| \cdot \left| J_0\left(2\frac{\Delta f_1}{f_0}\sin(\pi f_0 \tau_d)\right)\right|, \quad (8)$$

which shows that the synthesized coherence function in the double-modulation scheme is roughly given by the product of the coherence functions synthesized into a series of periodical delta-function-like peaks by each modulation frequency.

Based on Eq. (7), we simulated the synthesized coherence function when $m = 4$, as shown in Figs. 3(a)-3(c). The ratio of the modulation amplitudes (Δf_4 / Δf_1) was set to 10. In Fig. 3(c), the 1st, 2nd, 3rd, 5th, 6th, 7th, and 9th correlation peaks were suppressed, which shows that the measurement range was multiplied by 4 times while maintaining the spatial resolution.

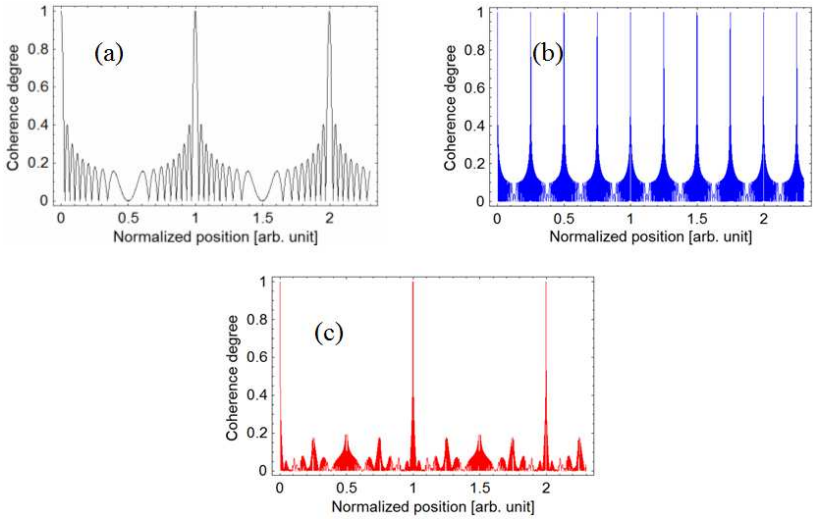

Fig. 3. Synthesized coherence functions with the modulation at (a) f_0 only, (b) $4f_0$ only, and (c) f_0 and $4f_0$.

4. Experiments

First, the effectiveness of the double-modulation scheme was experimentally shown. As the two modulation frequencies, f_0 and $5f_0$ were used (Δf_5 = 5.4 GHz), where f_0 was set to 68.481 kHz. According to Eqs. (1) and (2), the spatial resolution and the measurement range determined by the conventional single modulation at $5f_0$ were 53.1 cm and 302.1 m, respectively. An SMF of 1 km was used as the FUT, and about 0.15-% strain was applied to a 3-m section (990 – 993 m). The correlation peak was placed at the middle of the strain-applied section. The polarization state was optimized by adjusting polarization controllers so that the peak intensity of BGS without strain applied becomes maximal. Averaging was conducted 10 times to measure one BGS.

#121173 - $15.00 USD Received 8 Dec 2009; revised 1 Mar 2010; accepted 3 Mar 2010; published 10 Mar 2010

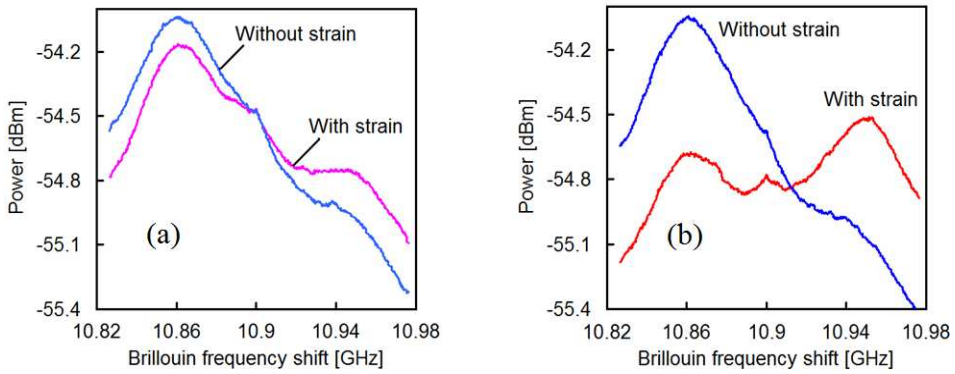

Fig. 4. Measured strain-dependences of BGS (a) without and (b) with double-modulation scheme.

Figure 4(a) shows the measured BGS with and without strain applied when the single modulation at $5f_0$ was applied. Since there were three correlation peaks within the FUT, the change of BGS was not observed as a clear shift of the peak. Here, a kink observed at 10.9 GHz was caused by range switching of the electrical spectrum analyzer (ESA). In contrast, Fig. 4(b) shows the measured BGS when the double-modulation scheme was employed. The applied strain was observed as a clear shift of the BGS peak. The remaining peak at about 10.86 GHz in the curve with strain applied, which can be regarded as noise, originates from the correlation sidelobes that were not completely suppressed. As long as this remaining peak is lower in power than the BGS peak, the measurement is performed correctly. In practical cases with two or more strains applied along the FUT, the power of the remaining peak becomes even smaller.

Then, the double modulation and the single modulation were compared in a distributed strain measurement. A strain of 0.15% was applied to a 90-cm section (990.0 – 990.9 m). With f_0 swept from 68.362 kHz to 68.497 kHz, BGS was measured every 5 cm. The other conditions were the same as those in the preceding experiment. The measured distributions of BGS and BFS with the single modulation at $5f_0$ (m = 5) are shown in Figs. 5(a) and 5(b), respectively. Although BGS slightly changed at the strain-applied section, a correct distribution of BFS was not acquired. On the other hand, the measured results in the double-modulation scheme with f_0 and $5f_0$ are shown in Figs. 6(a) and 6(b). The strain-applied 90-cm section was correctly detected. The measurement accuracy in this experiment was about +/– 7 MHz, corresponding to about +/– 120 με. The ratio N_R was 2845 (= 1.51 km / 53.1 cm), which is much higher than 1515 obtained previously in the temporal gating scheme.

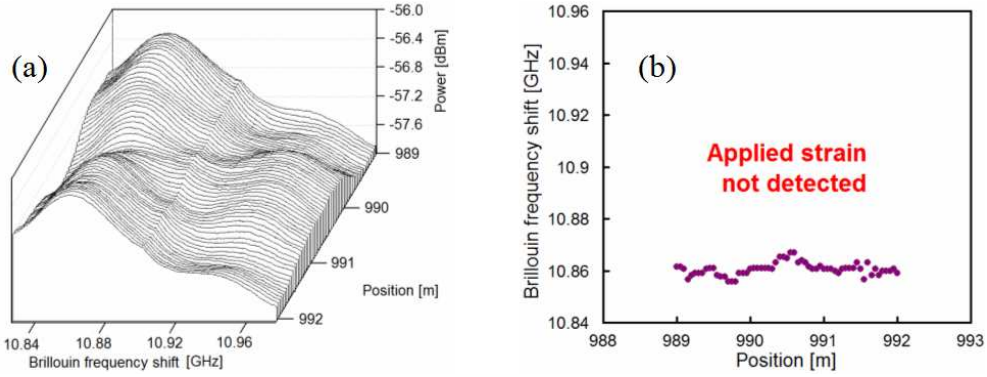

Fig. 5. Measured distributions of (a) BGS, and (b) BFS when the double-modulation scheme was not employed.

#121173 - $15.00 USD Received 8 Dec 2009; revised 1 Mar 2010; accepted 3 Mar 2010; published 10 Mar 2010

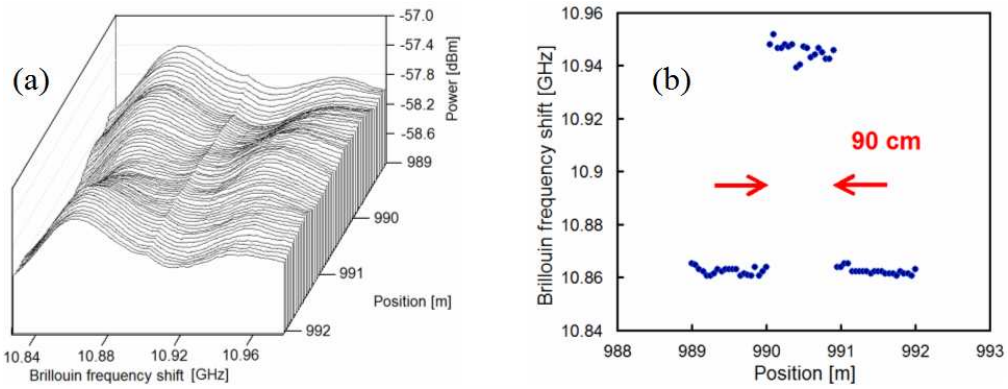

Fig. 6. Measured distributions of (a) BGS, and (b) BFS when the double-modulation scheme was employed (N_R = 2845).

The upper limit of m is determined by noise floor of the ESA, polarization state, FUT length, nonlinear dependence of LD frequency, *etc*. As m is increased, the S/N ratio is deteriorated due to the following two reasons: (i) the remaining peak (noise) in Fig. 4(b) becomes larger; (ii) the spatial resolution becomes higher, which accompanies the reduction of the BGS signal power. The second reason also deteriorates the measurement accuracy.

Finally, the double-modulation scheme was implemented with f_0 and $10f_0$ (Δf_{10} = 5.4 GHz) using a noise-floor compensation technique [15]. A strain of 0.15% was applied to a 40-cm section (990.0 – 990.4 m). With f_0 swept from 68.362 kHz to 68.474 kHz, the spatial resolution and the measurement range were 26.5 cm and 1.51 km, respectively, corresponding to N_R of 5690. The measured results are shown in Figs. 7(a) and 7(b). Although the S/N ratio was deteriorated compared to that in Fig. 6, the strain-applied 40-cm section was successfully detected. The measurement accuracy was about +/– 15 MHz, corresponding to about +/– 260 με. We think further research is needed to enhance the measurement accuracy by employing some methods such as those described in Refs [17]-[18].

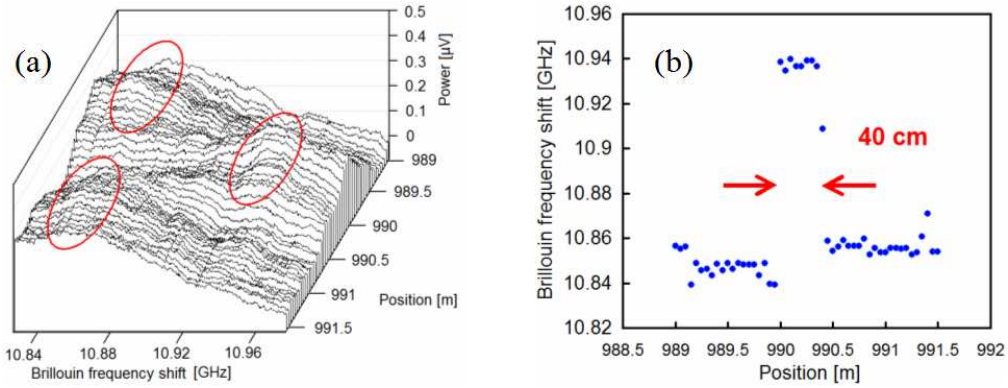

Fig. 7. Measured distributions of (a) BGS, and (b) BFS with the double-modulation scheme when the noise-floor compensation technique was employed (N_R = 5690).

5. Conclusion

In this paper, we developed a double-modulation scheme to mitigate the trade-off between the measurement range and the spatial resolution in BOCDR. In the experiment, 53-cm resolution and 1.5-km measurement range were simultaneously obtained. Furthermore, 27-cm resolution and 1.5-km measurement range were also simultaneously achieved when a noise-floor compensation technique was employed. We expect the double-modulation scheme will provide BOCDR with more feasibility as a fiber-optic nerve system in smart materials and structures.

#121173 - $15.00 USD Received 8 Dec 2009; revised 1 Mar 2010; accepted 3 Mar 2010; published 10 Mar 2010

Acknowledgments

The authors thank Mr. Koji Kajiwara at the University of Tokyo, Japan, for helpful discussions and comments. Yosuke Mizuno is grateful to the Japan Society for the Promotion of Science (JSPS) Research Fellowships for Young Scientists. This work was supported by the Grant-in-Aid for Scientific Research (S) and the Global Center of Excellence (G-COE) Program from the Ministry of Education, Culture, Sports, Science and Technology (MEXT), Japan.

#121173 - $15.00 USD Received 8 Dec 2009; revised 1 Mar 2010; accepted 3 Mar 2010; published 10 Mar 2010